High speed observations of ultrasonic fragmentation and de-agglomeration process of free-floating intermetallics and oxide particles

Abhinav Priyadarshi[*1], Tungky Subroto[2], Koulis Pericleous[3], Dmitry Eskin[2,4], John Durodola[1], Iakovos Tzanakis[1,5]

[1]Faculty of Technology, Design and Environment, Oxford Brookes University, Oxford, United Kingdom
[2]Brunel Centre for Advance Solidification Technology (BCAST), Brunel University London, Uxbridge, United Kingdom
[3]Computational Science and Engineering Group (CSEG), Department of Mathematics, University of Greenwich, London, United Kingdom
[4]Tomsk State University, Tomsk, Russia
[5]Department of Materials, University of Oxford, Oxford, United Kingdom

Abstract

The need for lightweight and high-strength advance materials in the form of metal-matrix composites with micron-sized particulate reinforcements has received considerable attention within automotive and aerospace industry. Ultrasonic melt treatment of Al-alloys offers a sustainable and eco-friendly approach to produce structural refinement through enhanced heterogeneous nucleation obtained from combined effect of sono-fragmentation of primary intermetallic/dendrites and de-agglomeration of non-metallic oxides/inclusions. However, owing to complexity of the process, understanding of the underlying mechanisms behind these effects is still rudimentary and lacks experimental evidences. In this paper, an insight into the underlying mechanism of fragmentation and de-agglomeration of Al_3Zr intermetallic and MgO oxide particles, respectively, in water is presented. Real-time high-speed imaging was performed to discern the dynamic interaction of cavitation with free-floating particles in a controlled ultrasonic environment. In-situ observations revealed that intermetallic breakage primarily occurs due to propagating shock waves, whereas the oxide de-agglomeration happens through microbubble cluster collapses close to the agglomerate.

Keywords: Ultrasonic cavitation melt treatment, de-agglomeration, intermetallics, oxides, fragmentation, high-speed camera

*Corresponding author
E-mail address: abhinav.priyadarshi-2018@brookes.ac.uk (Abhinav Priyadarshi)

1. Introduction

The production of metal matrix composites with improved material quality relies on the uniform homogeneous distribution and dispersion of micro and nano sized particles/reinforcements within the liquid metals [1]. This can be achieved using various external field melt processing techniques such as shearing, electromagnetic stirring and ultrasonic vibrations that can produce effective grain refinement of cast alloys. One of the applicable ways to attain this is through ultrasonic melt processing (USP). USP causes fragmentation and de-agglomeration of secondary phase particles/inclusions formed or present within the metallic melts [2] via the phenomenon of acoustic cavitation. Introduction of high intensity ultrasonic waves into the liquid metal promotes nucleation, growth and violent implosion of pre-existing gas and newly formed vapour bubbles. The collapsing bubble or bubbly clouds produce powerful shock waves and high-speed liquid jets generating large shear forces in the surrounding liquid region [3]. The resulting shear stresses, particularly on the nearby solid phase/surfaces has been found to have a damaging effect in terms of cavitation erosion, de-agglomeration and fragmentation [4–6]. However, the refinement and distribution of secondary fragmented/dispersed cluster of particles in liquid metals is due to the combined action from the generated cavitation and the primary and secondary cavitation flows (acoustic streaming) that disperse the broken fragments within the bulk liquid for further disintegration. In real Al melts, these solid phase particles can be either in the form of emerging intermetallic dendrites as primary crystals formed during solidification or the exogenous non-metallic inclusions as oxides. USP has shown to promote heterogeneous nucleation within the solidifying melt through effective wetting of these particles to act as active substrate of grain nucleation. Since these particles are often found to occur in free-floating condition, the mechanism through which the fragmentation and de-agglomeration transpire is largely unknown and is dominated by problems of opacity and working temperatures of Al melts.

To overcome these imposed restrictions, water has been established as a suitable transparent analogue medium

for such studies that closely replicates the cavitation behaviour in liquid Al [2, 7–9]. Very few studies have been performed until now to contemplate the associated effects of cavitation in such multi-phase systems. Wang et al. [7] were first to identify the cavitation-induced fragmentation of various primary intermetallics formed in Al alloys. Recent studies [6, 8, 9] have reported that the main driving force of crystal fragmentation is the emitted shock waves that produces tensile and shear stresses causing its brittle fracture though the fatigue related mechanism. However, these studies were made specifically for fixed crystals. In conventional USP, the primary intermetallics are found to be freely-floating within the Al melts. Therefore, studying the sono-fragmentation of such particles is of prime importance to achieve thorough understanding of the underlying mechanisms. On the contrary, the studies concerning de-agglomeration of oxides is even scarce. Majority of those investigations have been performed in ex-situ conditions where the de-agglomeration effects were interpreted through post-mortem microstructural observations of dispersed oxide particles. Previous study on the ultrasonic de-agglomeration of TiB_2 clusters in an AlTiB master alloy showed that induced cavitation led to formation of micron sized TiB_2 particles with sizes ranging between 1-3 μm [10]. These individual particles then act as active heterogeneous nucleation site for development of Al grains. However, there was no information presented regarding the process mechanism that leads to particle de-agglomeration. Eskin et al. [2] recently discovered that the de-agglomeration of MgO aggregates initiated from outside surface and the oscillating cavitation bubble eroded the oxide particles through 'chipping-off'of individual particles. Nonetheless, the complete mechanism of de-agglomeration from the onset of cavitation and role of gas/vapour bubbles has barely been visualised until now and presents a large gap in the literature. Moreover, the existing knowledge of the overall ultrasonic de-agglomeration process is mostly conceptual and is not yet validated with experiments. This calls for the need for investigation.

Therefore, the present work aims to fill in this knowledge gap by looking onto the fragmentation and de-agglomeration process of free-floating primary crystals (Al_3Zr) and oxide (MgO) agglomerates separately in de-ionised water under the influence of power ultrasound. The in-situ high-speed filming was performed to reveal the interaction of these solid phases with the induced acoustic cavitation and streaming responses.

2. Experimental methodology

The primary Al_3Zr crystals were extracted from an Al-3 wt% Zr alloy matrix. The intermetallic extraction procedure has been discussed elsewhere [8]. Intermetallic crystals with sizes in the range of 5-6 mm and thickness varying between 60-70 μm were used for the fragmentation experiments. A single crystal was deployed in a transparent vessel of dimensions, L: 25 mm, W: 10 mm, H: 45 mm containing de-ionised water filled up to a height of 25 mm and was allowed to settle down. The liquid was then subjected to ultrasonic excitation under room temperature conditions using a piezoelectric transducer operating at 24 kHz coupled with a tapered titanium horn having a tip diameter of 3 mm. The horn tip was submerged 10 mm below the liquid surface with tip-vibration amplitude of 210 μm peak to peak. In-situ observation of crystal fragmentation was undertaken using a Photron SA-Z high-speed camera combined with a 12× Navitar zoom adapter lens. The images sequence were captured at a resolution of 640 × 512 pixels with frame rates up to 100,000 fps. The background illumination was provided from a high intensity Multi LED flash lamp. For de-agglomeration experiments, MgO agglomerates with particle size in the range of 0.5 – 10 μm were employed. In this case, the sonotrode tip was positioned at a distance of 3.5 mm above the agglomerates and the cavitation-induced de-agglomeration was sequenced at a frame rate of 50 kfps. Contrary to the intermetallic fragmentation, here the illumination was provided from the front of the imaging plane using a combination of Multi LED flash lamp and Fibre Optic Haloid lamp. The experimental setup has been schematically illustrated elsewhere [11]. Figure 1 shows the scanning electron microscope images of the Al_3Zr crystal and MgO agglomerate prior to ultrasound exposure. The ultrasound-induced breakup sequences were recorded for five similar size crystals and agglomerates for repeatability of the observations. Only most illustrative sequences of images have been described in this paper.

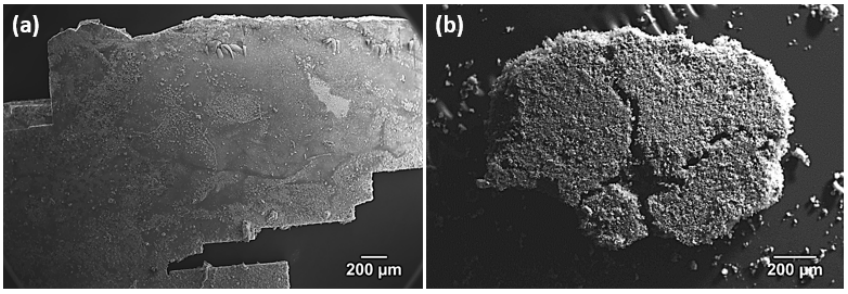

Figure. 1. Microstructural images showing the surface morphology of (a) extracted Al_3Zr crystal and (b) MgO agglomerate.

3. Results and Discussion

3.1 Intermetallic fragmentation

Figure 2 displays the series of in-situ images captured frame-by-frame that illustrate the sono-fragmentation response of a free-floating crystal having dimension of approximately L: 5.5 mm × W: 3.3 mm × T: 0.06 mm. Figure 2a shows the floating intermetallic crystal being driven towards the horn tip caused by the ultrasonic-induced streaming flow (t = 0 ms). As soon as the crystal reached close to the source (t = 4 ms), instant fracture occurred causing it to break apart (Figure 2b). The crystal further fractured into multiple small fragments (see Figure 2c) as it passed through the collapsing cavitation cloud beneath the horn tip where the shock wave intensity is strongest as we have recently shown in [12]. Consequently, the broken crystals were pushed into the bulk liquid by the streaming jet causing them to recirculate along the marked direction (t = 81 ms). During the recirculation, some of the crystal re-fragmented while some passed the cavitation cloud unaffectedly. For example, crystal marked as 'A' in Figure 2d underwent further breakage as it recirculated back to the source (Figure 2e). On the contrary, the fragment marked as 'B' did not suffer any breakage while passing the cavitation zone for the first time as shown in Figure 2f. After around 210 ms, at t = 408 ms, the crystal 'B' fragmented while coming in close proximity of the sonotrode tip during the subsequent recirculation cycle. The time taken by the crystal to complete a full flow cycle will depend on the recirculation path determined by the acquired momentum from the strong cavitation collapses occurring near the sonotrode tip. The flow speed of the fragments after interaction with the cavitation cloud reached up 2 m/s. Nonetheless, it is definite that every fragment will follow some sort of flow pattern and will pass the cavitation zone several times during their recirculation. Figure 2(g-h) also shows many vigorously oscillating microbubble clusters within the flow field continuously splitting and coarsening while undergoing shape fluctuations. These bubble clusters were also seen to attach with the floating fragments and move against the streaming flow as shown in Figure 2 (i-j). It should be noted that during these observations the attached clusters did not produce any fragmentation of the crystal. The crystal fragmentation process kept repeating and producing numerous fragments of smaller sizes as they crossed the cavitation zone (Figure 2 (k-l)). Thus, it is apparent from these sequences of images that the cavitation-induced acoustic streaming generates localised flow of the intermetallic crystal driving them back to the source for further treatment. The cavitation environment is expected to be more aggressive in the case of liquid Al assuming the acoustic flow behaviour bears similarity to that of water [2]. The crystal breakdown is also likely to be faster in Al melts as the induced acoustic pressure is about 4 times higher than those observed in case of water [13]. Moreover, owing to large density of Al melt, the fast sedimentation of primary crystals can further be suppressed expediting the fragmentation response. This justification is, however, established based on the initial results and more research is required including the mechanical behaviour of intermetallics at higher temperatures i.e. up to 700°C (currently unknown), in order to confirm this trend. It has been reported that the fragmented intermetallics can also act as an active heterogeneous substrate for further nucleation of Al dendrites/grains promoting microstructural refinement within the solidified cast alloy [14]. To reveal the precise fragmentation mechanism of these intermetallics under the influence of ultrasound, we conducted another set of imaging experiments at a higher frame rate by focussing on the region closer to the sonotrode tip (as identified from the low frame rate experiments as the primary area where fragmentation occurs).

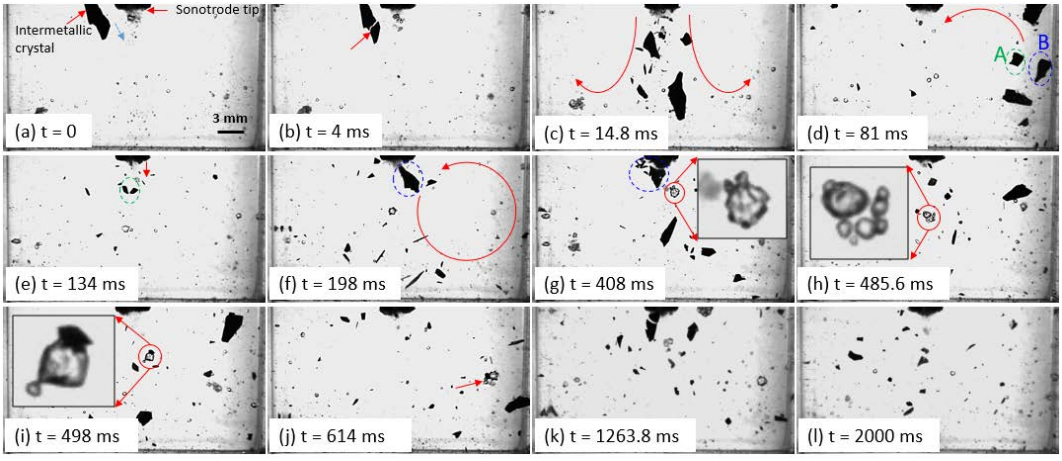

Figure. 2. Sequence of in-situ real-time high-speed images demonstrating the fragmentation process of a single Al_3Zr particle captured at 5k fps with sonotrode amplitude operating at a 210 μm peak-to-peak amplitude.

Figure 3 shows the zoomed image sequence of the crystal fragmentation occurring close to the sonotrode tip under a low frequency and high amplitude power ultrasound. Figure 2a shows the horn tip with cavitation cloud under the collapsed condition. With the inception of cavitation, the developed recirculation convective flow pushed the intermetallic towards the ultrasonic source (Figure 2b). As the crystal came closer to the vibrating source, the cavitation cloud beneath the horn tip started to undergo violent collapses. The oscillating frequency of the cavitating cloud was dropped to almost 5 kHz (subharmonic to the driving frequency). Figure 2c at t = 1.76 ms shows the instant when the floating crystal comes in contact with the developed cloud (marked with an arrow). Upon subsequent cavitation collapses, the crystal underwent severe bending, with fluctuation matching the cloud oscillating frequency. After 5 such consecutive cloud collapses, crack initiation occurred across the crystal surface (marked with rectangular box) as depicted in Figure 2d. At t = 2.82 ms, the crack fully propagated with complete fragmentation at t = 2.92 ms (Figure 3 (e-f)). 2nd breakage occurred as the crystal moved underneath the sonotrode tip causing further disintegration as shown in Figure 3 (g-h). The induced acoustic flow then pushed the fragments into the bulk liquid. As a result of recirculating flow, a fragmented crystal from the bulk was found to move towards the source eventually breaking down into multiple smaller fragments (Figure 3 (i-l)). The fragmentation process observed in this image sequence was most likely governed by the shock wave emissions produced from the subharmonic collapses of the bubble cloud attached to the horn tip that caused repetitive bending of the crystal until it fractured [8]. These subharmonic signals possess very high strength with their intensity even reaching up to the level of the ultrasonic driving pressure wave [15]. It has been reported that these subharmonic signals generated by the acoustically induced cavitation implosions are associated with periodic shock wave emissions [16, 17]. Moreover, the vulnerability of these crystals to fail instantaneously upon shock wave exposure is related with their extremely brittle behaviour with fracture toughness close to 1 MPa√m. It has been previously shown that the sono-fragmentation of intermetallics occurs via low cycle fatigue mechanism, where the shock pressure triggers a pre-existing sub-critical crack to reach a critical length, ultimately leading to brittle fracture in just a few acoustic cycles [8].

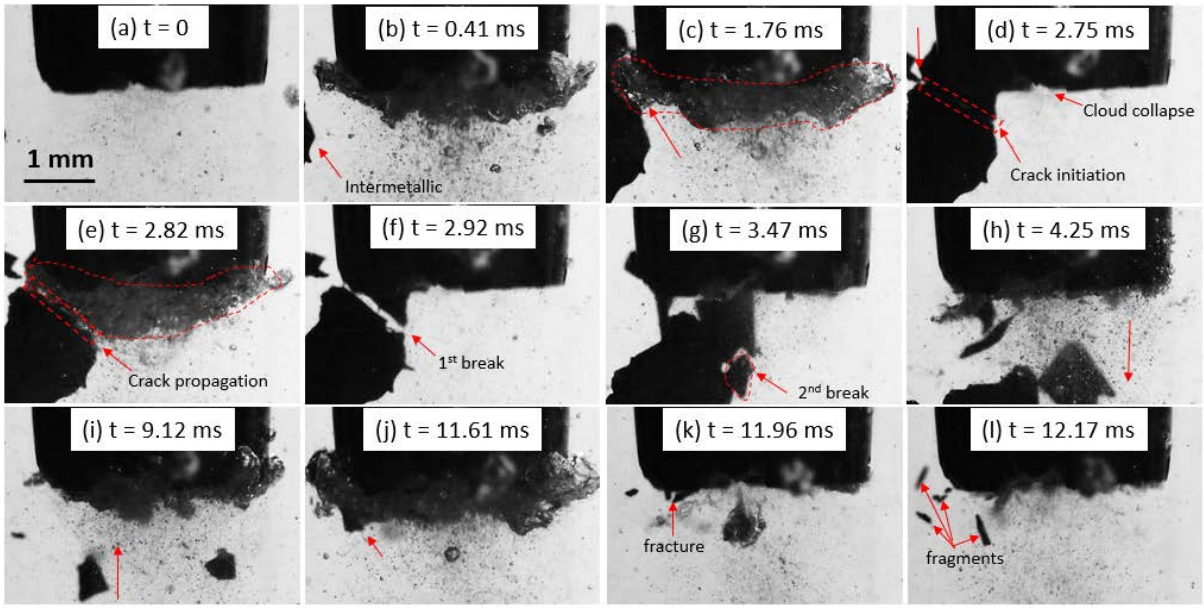

Figure. 3. Sequence of in-situ real-time high-speed images near the sonotrode tip showing the fragmentation process of Al_3Zr particle captured at 100k fps with sonotrode amplitude operating at a 210 μm peak-to-peak amplitude.

3.2 Oxide de-agglomeration

Figure 4 outlines the sequence of high-speed images displaying the de-agglomeration process of MgO aggregates under the influence of ultrasonic cavitation. The first frame at t = 0 shows the two agglomerates of sizes in the range of 600-650 μm with gas microbubbles (shown as inset) present on its surface and the surrounding walls of the cuvette (Figure 4a). The introduction of ultrasonic signal within the liquid at t = 3.56 ms, triggered these gas bubbles to oscillate and move towards the nearby agglomerate (marked with yellow arrows) as shown in Figure 4b. With the increase in the cavitation activity at the tip of the ultrasonic horn, the oscillating gas bubbles underwent splitting and coalesced with other bubbles to develop into microbubble clusters of size approximately

300 μm in diameter as shown in Figure 4c. The vigorous pulsation of these microbubble clusters adjacent to the aggregate initiated the 'chipping-off' of individual particles from the surface (marked with yellow arrows) as seen in Figure 4d. As the cavitation stream reached the base of the cuvette, the chaotically oscillating microbubble clusters further expedited the de-agglomeration from within the oxide making the aggregate loose (Figure 4e). At time, t = 10.42 ms, the bubble cloud stream surrounded the agglomerate intensifying the de-agglomeration process as shown in Figure 4f. The large imploding bubble clusters produced subsequent breakage of the aggregates (see inset of Figure 4g) and the induced recirculating vortex formed at the sides of the cavitation stream (marked with blue arrows) dispersed the de-agglomerated oxide particles into the bulk liquid as shown in Figure 4(f-i). It is evident from this sequence of images that the de-agglomeration transpires primarily by the intensified acoustic flow and the formation and collapse of bubble clusters in the vicinity of aggregates leading to removal of oxide particles from the surface. To better understand and resolve the de-agglomeration process occurring from within the aggregate, a separate imaging experiment was performed using a single MgO aggregate.

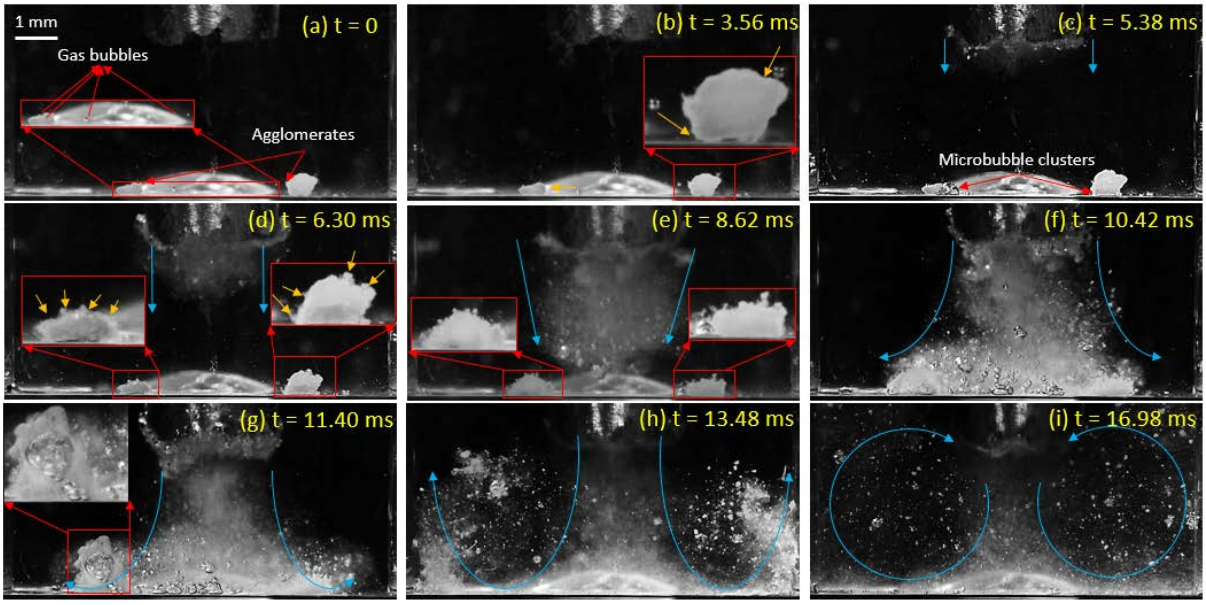

Figure. 4. Sequence of in-situ real-time high-speed images illustrating the de-agglomeration process of MgO aggregates captured at 50k fps with sonotrode amplitude operating at a 210 μm peak-to-peak amplitude.

Figure 5 displays the series of images with zoomed in view of the agglomerate positioned ~3.5 mm away from the horn tip. Figure 5a shows a non-spherical MgO agglomerate of size approximately 1.8 mm with pre-existing gas bubble underneath (marked with a red arrow). These oxides are highly porous in nature making them an ideal site for bubble nucleation. After the ultrasound device was switched on, the micro gas bubbles present started to undergo pulsations (Figure 5b). At t = 7.58 ms, with increased bubble oscillations, the microbubbles present within the agglomerate grew in size even bulging out from the surface (marked with an arrow). Interestingly, the breakage of the agglomerate also occurred possibly owing to the tensile stresses as the bubble expanded and collapsed as shown in the marked region in Figure 5c. The continued dynamic rebound and implosions of microbubble clusters led to complete desintegration of the aggregate (as marked with red arrows) as shown in Figure 5d. With the incoming cavitation cloud stream (marked with blue arrows) from the ultrasonic source reaching closer to the oxide, the oscillating microbubbles nearby caused the loosening of the aggregate from both the surface and the bulk (Figure 5e). There are two possible mechanism that could be responsible for this effect. Either the chaotically splitting bubbles in the vicinity triggered the tiny vapour bubbles existing as gas pockets within the micro-capillaries to volumetrically fluctuate, thereby pushing the oxide particles apart and resulting in agglomerate breakup; or the introduced acoustic wave produced adequate pressures that forced the surrounding liquid to enter into the micro-cavities inducing de-agglomeration by the ultrasonic capillary effect [18–20]. However, more research is required to clarify this hypothesis. As the cavitation bubble stream interacted the loosely bonded oxide particles, they were subsequently dispersed into the bulk liquid (resembling an avalanche) by the induced streaming flow as shown in Figure 5f.

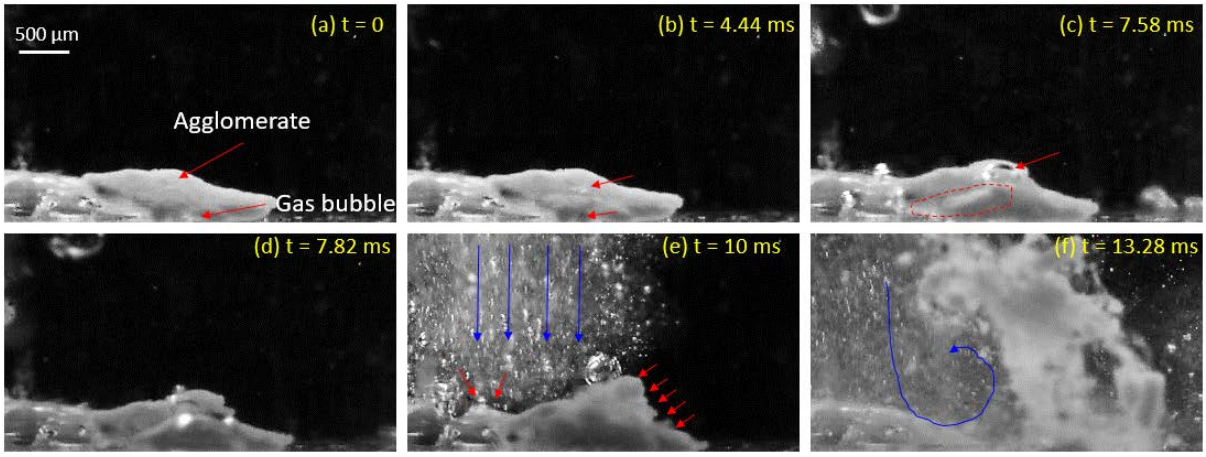

Figure. 5. Sequence of in-situ real-time high-speed images displaying the de-agglomeration process of single MgO aggregate captured at 50k fps with sonotrode amplitude operating at a 210 µm peak-to-peak amplitude.

4. Conclusions

The underlying fragmentation and de-agglomeration process of free-floating primary intermetallic crystals and oxide aggregates, respectively, under ultrasonic excitation in water were revealed using in-situ high-speed observations. Experimental evidence showed that the driving mechanisms behind the fragmentation and de-agglomeration are distinctively different. In the case of Al_3Zr, the fragmentation occurs through contactless interaction implying that the propagating shock waves emitted from the subharmonic cloud collapses occurring beneath the sonotrode tip are likely the governing mechanism of crystal fragmentation (as also previously observed in case of fixed intermetallics). The fragmented crystals are then brought back into the cavitation zone for further disintegration into smaller sizes by the recirculating streaming vortex of the acoustic flow. While in the case of MgO, the de-agglomeration transpires from the surface as well as the bulk. The particle erosion from the surface of the aggregate possibly happens through the particle chipping mechanism as a result of cavitation collapses occurring adjacent to oxide. In addition, the induced acoustic pressures from the oscillating micro-bubble pushes the oxide particle from within making the agglomerates loose. The acoustic streaming flow then disperses the loosely bonded particles into the bulk liquid. Understanding of these mechanisms is important for validation of numerical models and improving solidification technologies.

Acknowledgement

This work was financially supported by the UK Engineering and Physical Sciences Research Council (EPSRC) under the project UltraMelt2 (grant EP/R011001/1, EP/R011095/1 and EP/R011044/1).

References

1. Tamayo-Ariztondo J, Madam SV, Djan E, Eskin DG, Babu NH, Fan Z (2014) Nanoparticles Distribution and Mechanical Properties of Aluminum-Matrix Nano-Composites Treated with External Fields. TMS Light Met 1411–1415. https://doi.org/10.1007/978-3-319-48144-9_236

2. Eskin DG, Tzanakis I, Wang F, Lebon GSB, Subroto T, Pericleous K, Mi J (2019) Fundamental studies of ultrasonic melt processing. Ultrason Sonochem 52:455–467. https://doi.org/10.1016/J.ULTSONCH.2018.12.028

3. Leong T, Ashokkumar M, Kentish S (2011) The fundamentals of power ultrasound-A review. Acoust Aust 39: 54–63.

4. Dular M, Požar T, Zevnik J, Petkovšek R (2019) High speed observation of damage created by a collapse of a single cavitation bubble. Wear 418–419:13–23. https://doi.org/10.1016/j.wear.2018.11.004

5. Bałdyga J, Makowski Ł, Orciuch W, Sauter C, Schuchmann HP (2009) Agglomerate dispersion in cavitating flows. Chem Eng Res Des 87:474–484. https://doi.org/10.1016/j.cherd.2008.12.015

6. Priyadarshi A, Subroto T, Conte M, Prentice P, Pericleous K, Eskin D, Durodola J, Tzanakis I (2020) Ultrasound induced fragmentation of primary Al3Zr crystals. In: De Geuser F, Deschamps A, Ehrström

J-C, Jarry P, Salloum-Abou-Jaoude G, Salvo L, Sigli C (eds) MATEC Web of Conferences. EDP Sciences, 326: 04002. https://doi.org/10.1051/matecconf/202032604002

7. Wang F, Tzanakis I, Eskin D, Mi J, Connolley T (2017) In situ observation of ultrasonic cavitation-induced fragmentation of the primary crystals formed in Al alloys. Ultrason Sonochem 39:66–76. https://doi.org/10.1016/j.ultsonch.2017.03.057

8. Priyadarshi A, Khavari M, Subroto T, Conte M, Prentice P, Pericleous K, Eskin D, Durodola J, Tzanakis I (2021) On the governing fragmentation mechanism of primary intermetallics by induced cavitation. Ultrason Sonochem 70:105260 . https://doi.org/10.1016/j.ultsonch.2020.105260.

9. Priyadarshi A, Subroto T, Conte M, Pericelous K, Eskin D, Prentice P, Tzanakis I (2020) Nanoindentation and Cavitation-Induced Fragmentation Study of Primary Al_3Zr Intermetallics Formed in Al Alloys. In: Minerals, Metals and Materials Series. Springer, pp 168–173.

10. Eskin GI, Rukhman AA, Bochvar SG, Elfimov VY, Konovalov D V (2008) New developments in the technology of ultrasonic melt treatment in light alloys. Tsvetn Met 3:105–110.

11. Priyadarshi A, Bin Shahrani S, Subroto T, Pericleous K, Eskin D, Durodola J, Tzanakis I (2021) Ultrasonic cavitation erosion mechanism of free-floating Al3Zr intermetallics. In: 11th International Symposium on Cavitation (CAV2021). Daejon, Korea, pp 1–5.

12. Morton JA, Khavari M, Qin L, Maciejewska BM, Tyurnina A V., Grobert N, Eskin DG, Mi J, Porfyrakis K, Prentice P, Tzanakis I (2021) New insights into sono-exfoliation mechanisms of graphite: In situ high-speed imaging studies and acoustic measurements. Mater Today (in press). https://doi.org/10.1016/J.MATTOD.2021.05.005

13. Tzanakis I, Lebon GSB, Eskin DG, Pericleous K (2015) Comparison of cavitation intensity in water and in molten aluminium using a high-temperature cavitometer. J Phys Conf Ser 656: 012120. https://doi.org/10.1088/1742-6596/656/1/012120

14. Eskin D (2020) Ultrasonic processing of aluminium alloys above the liquidus: the role of Zr. In: MATEC Web of Conferences. EDP Sciences, 326:06002. https://doi.org/10.1051/matecconf/202032606002

15. Žnidarčič A, Mettin R, Cairós C, Dular M (2014) Attached cavitation at a small diameter ultrasonic horn tip. Phys Fluids 26:023304. https://doi.org/10.1063/1.4866270

16. Johnston K, Tapia-Siles C, Gerold B, Postema M, Cochran S, Cuschieri A, Prentice P (2014) Periodic shock-emission from acoustically driven cavitation clouds: A source of the subharmonic signal. Ultrasonics 54:2151–2158 . https://doi.org/10.1016/j.ultras.2014.06.011

17. Yusuf L, Symes MD, Prentice P (2021) Characterising the cavitation activity generated by an ultrasonic horn at varying tip-vibration amplitudes. Ultrason Sonochem 70:105273. https://doi.org/10.1016/j.ultsonch.2020.105273

18. Tzanakis I, Xu WW, Eskin DG, Lee PD, Kotsovinos N (2015) In situ observation and analysis of ultrasonic capillary effect in molten aluminium. Ultrason Sonochem 27:72–80. https://doi.org/10.1016/j.ultsonch.2015.04.029

19. Kudryashova O, Vorozhtsov S (2016) On the Mechanism of Ultrasound-Driven Deagglomeration of Nanoparticle Agglomerates in Aluminum Melt. JOM 68:1307–1311. https://doi.org/10.1007/s11837-016-1851-z

20. Kudryashova O, Vorozhtsov A, Danilov P (2019) Deagglomeration and coagulation of particles in liquid metal under ultrasonic treatment. Arch Acoust 44:543–549. https://doi.org/10.24425/aoa.2019.129269